Radiation patterns of acoustic phonons emitted by hot electrons in a quantum well

V. V. Mitin, G. Paulavičius, and N. A. Bannov[a)]
Department of Electrical and Computer Engineering, Wayne State University, Detroit, Michigan 48202

M. A. Stroscio
U.S. Army Research Office, P.O. Box 12211, Research Triangle Park, North Carolina 27709-2211

(Received 28 November 1995; accepted for publication 7 March 1996)

The acoustic phonon radiation patterns and acoustic phonon spectra due to electron–acoustic-phonon interaction in a double barrier quantum well have been investigated by solving both the kinetic equations for electrons and phonons. The acoustic phonon radiation patterns have strongly pronounced maximum in the directions close to the perpendicular to the quantum well direction. The radiation pattern anisotropy is explained in terms of possible electron transitions, electron distribution function, and the Hamiltonian of electron–phonon interaction. It was shown that, the simple assumption that emitted phonons always have a perpendicular wave-vector component of the order of $2\pi/a$, where a is the width of the quantum well, cannot explain the strong anisotropy of the radiation patterns. More detailed analysis is required and has been carried out. The emitted acoustic phonon spectra have maxima at energies $2\pi\hbar u/a$, where u is the sound velocity. © *1996 American Institute of Physics.* [S0021-8979(96)02512-1]

I. INTRODUCTION

Electron interactions with acoustic phonons in low dimensional (LD) structures at low lattice temperatures play important roles in many kinetic phenomena. They determine the low–field electron mobility and the electron energy loss rate at low lattice temperatures. Hot acoustic phonon emission represents one of the significant channels for thermal energy removal from LD electron gases. The detection of acoustic phonons emitted by hot electrons provides a valuable tool for the investigation of electron–phonon interactions in heterostructures.

The problem of diagnosing acoustic phonons emitted by quasi-two–dimensional and one–dimensional electrons has attracted considerable attention during the last decade. It has been studied both experimentally[1–8] and theoretically.[9–15] In experiments,[1–8] the energy flux of acoustic phonons has been measured by bolometers, deposited on the opposite (with respect to the quantum well) side of the semiconductor substrate. Theoretical analysis[9–15] explains many features of the experimental results. However, of all these papers studied the acoustic phonon flux for the case when the distribution function of electrons is the Fermi function (or the Maxwell function). We formulate the problem of acoustic phonon emission in terms of the kinetic equations for both phonons and electrons allowing for in-plane heating electric field and nonequilibrium electrons. We have solved the kinetic equation for quasi two–dimensional electrons and obtained the electron distribution function. This function has been used to study the acoustic phonon energy flux due to acoustic phonon emission by hot electrons. We have investigated dependencies of the radiation patterns and the emitted acoustic phonon spectra on the applied electric field and obtained new interesting features in the acoustic phonon emission. In addition, in contrast to Refs. 9 and 12 we have taken into account the stimulated phonon emission processes. Our treatment is based on solving the quantum kinetic equation for phonons as was done in Refs. 9 and 12. However, we have formulated the boundary conditions for the energy fluxes in a clear integral form based on energy flux balances.

As it has been understood previously,[1,2,9,15] the radiation patterns of acoustic phonons have well-pronounced maxima inside the solid angle close to the normal to the quantum well (QW) direction (z-direction). These orientational dependencies are related to the quantum confinement of electrons in the quantum well and uncertainty in the conservation of the z-component of phonon wave vectors. In the case of QW structures, the emitted acoustic phonons have wave vectors with z-components, q_z, of the order of $2\pi/a$, where a is the width of the electron lateral confinement. For a 100 Å wide quantum well, $q_z \approx 6\times10^6$ cm^{-1}. At the same time, an electron with an energy of 40 meV in GaAs emits phonons with in-plane wave vector components about 6×10^6 cm^{-1}, for the case when the electron scatters in the direction, which is opposite to the direction of its initial motion. Therefore, the uncertainty in the phonon z-component conservation can explain only moderate anisotropy of acoustic phonon radiation patterns. We give another explanation for the strong anisotropy of the angular dependence of the differential acoustic phonon energy flux. We have also calculated the energy spectrum of nonequilibrium acoustic phonons radiated from such quantum well nanostructures as well as the electron energy loss rates in such structures.

In the next section, we will consider the problem at hand for a sample double heterostructure with geometry close to those used in experiments.[1,3–6] We will also define the differential energy flux and other measurable quantities related to acoustic phonon emission, which are relevant to this geometry. In the following section we will formulate the prob-

[a)] Present address: Box 7911, Department of Electrical and Computer Engineering, North Carolina State University, Raleigh, NC 27695-7911; Electronic mail: bannov@ecehlt1.ece.ncsu.edu

lem of phonon kinetics in terms of appropriate quantum kinetic equations. Then these equations will be transformed to a form which takes into account the geometry of the sample and the equation for the differential energy flux will be obtained. The last section reports results from numerical simulations and discusses physical interpretations of the radiation patterns and phonon spectra presented in this paper.

II. GEOMETRY AND THE MEASURABLE QUANTITIES

We will consider a double-barrier heterostructure quantum-well of width a bounded by planes $z=a/2$ and $z=-a/2$. The Cartesian coordinates x and y refer to the plane of the quantum well, the axis x is going in the direction of the average electron velocity, the y-axis augments the x- and z-axes to form a right-handed basis. Accordingly, the electric field, $\mathbf{E}$, is going in the direction of negative x. The dimensions of the quantum well in the $x-y$ plane are L_x and L_y. The acoustic phonons are detected by sensors located at a surface of the substrate. We assume that the distance, d, from the quantum well to the surface is large in comparison with the lateral dimensions of the quantum well: $d \gg L_x, L_y$; in this limit, the quantum well represents a point source of acoustic phonons. The described geometrical configuration corresponds to those of Refs. 5 and 6 as well as those of other experiments.

We define measurable quantities related to acoustic phonon emission by a point source; these include: the differential energy flux $\mathscr{G}(\hbar\omega,\Omega)$, the radiation pattern, $\mathscr{G}_{\hbar\omega}(\Omega)$, and the spectrum of acoustic phonons, $\mathscr{G}_{\Omega}(\hbar\omega)$. The energy flux density of acoustic phonons, $\Delta\mathbf{g}$, is defined as

$$\Delta\mathbf{g}=\frac{1}{8\pi^3}\int_{\Delta\mathbf{q}} d\mathbf{q}\mathbf{u}_{\mathbf{q}}\hbar\omega_{\mathbf{q}}N_{\mathbf{q}}(\mathbf{r}).$$

Here $N_{\mathbf{q}}$ is the phonon occupation number, e.g., the Planck function, $\hbar\omega_{\mathbf{q}}$ is the phonon energy, and $\mathbf{u}_{\mathbf{q}}$ is the phonon group velocity. The units for $\Delta\mathbf{g}$ are the energy per unit time, per unit area. The symbol Δ in $\Delta\mathbf{g}$ refers to the volume $\Delta\mathbf{q}$ of integration. The energy flux of acoustic phonons, ΔG, through a given surface, S, is defined by the formula

$$\Delta G=\int_S d\mathbf{S}\Delta\mathbf{g}=\frac{1}{8\pi^3}\int_{\Delta\mathbf{q}} d\mathbf{q}\int_S d\mathbf{S}\mathbf{u}_{\mathbf{q}}\hbar\omega_{\mathbf{q}}N_{\mathbf{q}}(\mathbf{r}).$$

We assume a simple linear isotropic dispersion relation $\omega_{\mathbf{q}}=uq$ and a simple formula for phonon group velocity $\mathbf{u}_{\mathbf{q}}=u\mathbf{q}/q$. Then ΔG is given by the formula

$$\Delta G=\int_{\Delta(\hbar\omega)} d(\hbar\omega)\int_{\Delta\Omega} d\Omega\,\mathscr{G}(\hbar\omega,\Omega), \tag{1}$$

where $\mathscr{G}(\hbar\omega,\Omega)$ is the differential energy flux (the phonon energy passing through a surface S per unit time, per unit solid angle, per unit energy interval), determined by the formula

$$\mathscr{G}(\hbar\omega,\Omega)=\frac{1}{8\pi^3}\int_S d\mathbf{S}\frac{\mathbf{q}}{q}uq^3N_{\mathbf{q}}(\mathbf{r}).$$

We will measure the differential energy flux in the units $(\text{ps sr})^{-1}$. In numerical Monte Carlo calculations, it is convenient to normalize the differential energy flux per one electron. The radiation pattern and the spectrum of acoustic phonons are defined as

$$\mathscr{G}_{\hbar\omega}(\Omega)=\int_0^\infty \mathscr{G}(\hbar\omega,\Omega)d(\hbar\omega),$$

$$\mathscr{G}_{\Omega}(\hbar\omega)=\int_{4\pi} \mathscr{G}(\hbar\omega,\Omega)d\Omega,$$

respectively. It is worth mentioning, that the differential energy flux detected by sensors on a surface of the semiconductor substrate is strongly modified by focusing due to the elastic anisotropy of crystal lattices. The directions of the phonon phase velocity (which is determined by the phonon wave vector) and the group velocity (which defines the direction of energy flow) differ in anisotropic crystals. This results in an increase of energy flow along some directions and a decrease along other directions in real space. If the differential energy flux of the source and the dispersion relationship for phonons is known, energy flow detected by sensors may be calculated through curvatures of surfaces of equal phonon energy (see, e.g., a review in Ref. 16). Because this task is quite laborious from a practical point of view, computer programs have been developed to calculate incoming energy to a detector energy flow allowing for a realistic geometry of the source of phonon radiation.[17]

III. THE PHONON KINETIC EQUATION

The problem at hand may be described by the kinetic equations for electron and phonon density matrices, $f_{k,k'}$ and $\sigma_{q,q'}$, in which electron–phonon interactions are taken within the second order of the perturbation theory. The indices k and q describe complete sets of electron and phonon quantum numbers: $k=(\mathbf{k}_\parallel,n)$, $q=(\mathbf{q}_\parallel,q_z)$. We will use these simple indices despite the obvious possibility of confusion with absolute values, because they significantly simplify and shorten formulae. If we need an absolute value of some vector, we will designate such quantities through the use of two vertical lines as in $|\mathbf{k}_\parallel|$ for example. The kinetic equation for the phonon density matrix has the following form:

$$\frac{\partial\sigma_{q,q'}}{\partial t}+i(\omega_q-\omega_{q'})\sigma_{q,q'}=\mathscr{J}_{ph-e}+\mathscr{J}_{ph-ph}, \tag{2}$$

where $\mathscr{J}_{ph-e}$ and $\mathscr{J}_{ph-ph}$ denote terms for phonon–electron and phonon–phonon interactions respectively.

The phonon–electron collision integral is given by the formula

$$\begin{aligned}\mathscr{J}_{ph-e}=&-\frac{i}{\hbar}\sum_{k,k',Q}\frac{w(k,k',q')w^*(k,k',Q)}{\varepsilon_k-\varepsilon_{k'}+\hbar\omega_q-i\lambda}\\&\times[(1-f_k)f_{k'}\delta_{q,Q}+(f_{k'}-f_k)\sigma_{q,Q}]\\&+\frac{i}{\hbar}\sum_{k,k',Q}\frac{w(k,k',Q)w^*(k,k',q)}{\varepsilon_k-\varepsilon_{k'}+\hbar\omega_{q'}+i\lambda}\\&\times[(1-f_k)f_{k'}\delta_{Q,q'}+(f_{k'}-f_k)\sigma_{Q,q'}].\end{aligned} \tag{3}$$

In the above equation, index Q denotes the phonon variables, $\lambda \to +0$. We have taken into account that electron gas is homogeneous in the $x-y$ plane and the electron intersubband transitions are significantly slower than the intersubband transitions; therefore, the electron density matrix is diagonal: $f_{k,k'} = \delta_{k,k'} f_k = \delta_{k,k'} f_{n,\mathbf{k}_\parallel}$. In our numerical calculations, we will consider only the case of strong electron lateral confinement, when only the lowest subband is occupied, therefore, the above assumptions are held. The matrix element, $w(k,k',q)$ determines the rate of electron–phonon scattering. We take the Hamiltonian of the electron–acoustic phonon interaction in the standard form,

$$H_{e-ph} = \sum_{\mathbf{q}} (\chi_{\mathbf{q}}(\mathbf{r}) b_{\mathbf{q}} + \chi^*_{\mathbf{q}}(\mathbf{r}) b^\dagger_{\mathbf{q}}),$$

where $\chi_{\mathbf{q}}$ gives the strength of the electron–acoustic phonon interaction, and $b_{\mathbf{q}}$ and $b^\dagger_{\mathbf{q}}$ are the destruction and creation operators respectively. For the system under consideration, $\chi_{\mathbf{q}}(\mathbf{r}) = \exp(i\mathbf{qr})\Gamma_{\mathbf{q}}$. With this notation, the matrix element, $w(k,k',q)$, is given by the formula

$$w(k,k',q) = \langle \mathbf{k}'_\parallel, n' | \chi_{\mathbf{q}} | \mathbf{k}_\parallel, n \rangle = \delta_{\mathbf{k}_\parallel + \mathbf{q}_\parallel, \mathbf{k}'_\parallel} \Gamma_{\mathbf{q}} \langle n' | \exp(iq_z z) | n \rangle.$$

For the case of the deformation potential interaction, which makes the major contribution to electron scattering by acoustic phonons

$$\Gamma_{\mathbf{q}} = \Gamma_q = \sqrt{\frac{\hbar}{2\rho \mathscr{V}_{pr} \omega_q}} i E_a q,$$

where E_a is the acoustic deformation potential constant, ρ is the crystal density, and $\mathscr{V}_{pr}$ is a principal volume. Because electrons do not interact with transverse acoustic phonons through the deformation potential, we have not included the phonon mode index in the phonon variables. Accordingly, $\omega_q = uq$ is the phonon dispersion relation for longitudinal phonons and u is the longitudinal phonon velocity.

We will need the overlap integral, $\mathscr{I}(n',n,q_z) = |\langle n' | \exp(iq_z z) | n \rangle|^2$. For the case of electron wave functions for an infinitely-deep rectangular quantum well, the overlap integral may be calculated analytically. It takes the form

$$\mathscr{I}(n',n,q_z) = \frac{32(n'n\tilde{q})^2 [\,1-(-1)^{n+n'}\cos\pi\tilde{q}\,]}{\pi^2 [\tilde{q}^{\,4} - 2(n'^2+n^2)\tilde{q}^{\,2} + (n^2-n'^2)^2]^2},$$

where $\tilde{q} = aq_z/\pi$. The function $\mathscr{I}(n',n,q_z)$ for electrons in the lowest subband ($n = n' = 1$) is shown on Fig. 1. From Fig. 1 it follows, that typical values of q_z for acoustic phonons interacting with electrons in QW are approximately equal to $2\pi/a$.

The electron density matrix (distribution function), $f_{n,\mathbf{k}_\parallel}$, satisfies the corresponding kinetic equation which takes into account the interaction of electrons with acoustic phonons as well as with optical phonons.

IV. DIFFERENTIAL ENERGY FLUX

We will use the phonon distribution function, $N_{\mathbf{q}}(\mathbf{r})$, defined by the Fourier transform

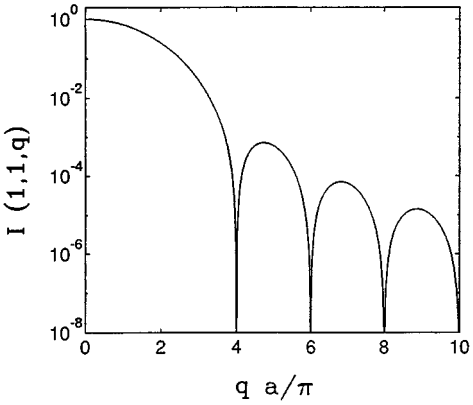

FIG. 1. The overlap integral $\mathscr{I}(1,1,q)$ for electron transitions inside subband number one.

$$N_{\mathbf{q}}(\mathbf{r}) = \sum_{\Delta\mathbf{q}} \sigma_{\mathbf{q}+\Delta\mathbf{q}/2, \mathbf{q}-\Delta\mathbf{q}/2} \exp(i\Delta\mathbf{qr}). \tag{4}$$

If we apply the Fourier transform defined by Eq. (4) to the phonon kinetic equation given by Eq. (2), we obtain the following equation

$$\frac{\partial N_{\mathbf{q}}(\mathbf{r})}{\partial t} + \mathbf{u}_{\mathbf{q}} \frac{\partial N_{\mathbf{q}}(\mathbf{r})}{\partial \mathbf{r}} = J_{ph-e} + J_{ph-ph}, \tag{5}$$

where $\mathbf{u}_{\mathbf{q}} = \partial\omega_{\mathbf{q}}/\partial\mathbf{q}$, and the collision integrals J_{ph-e} and J_{ph-ph} are the Fourier transforms of the collision integrals $\mathscr{J}_{ph-e}$ and $\mathscr{J}_{ph-ph}$, respectively. We have used the fact that $N_{\mathbf{q}}(\mathbf{r})$ is a slowly varying function of coordinates in the left hand side of Eq. (5) and neglected the derivatives of $\omega_{\mathbf{q}}$ and $N_{\mathbf{q}}(\mathbf{r})$ over $\mathbf{q}$ and $\mathbf{r}$ respectively of the third, fifth, and higher orders.

When making estimates for the acoustic phonon propagation and their interactions with electrons, it is convenient to treat them as wave packets of finite size, Δr, and, accordingly, of finite width in the phase space, Δq. A typical energy for acoustic phonons emitted by quasi-two-dimensional electrons, as is shown below, is equal to about $2\pi\hbar u/a$; for usual material and quantum well parameters (GaAs quantum well 100 Å wide) it is equal to about 2 meV. A typical wavelength of acoustic phonons emitted by quasi-two–dimensional electrons, λ, is equal to a; so for our estimate $\lambda \approx 100$Å. Therefore, it is reasonable to take $\Delta r = 10a$ or larger. At the same time, we assume, that the in-plane dimensions of the quantum well are much larger than Δr: $\Delta r \ll L_x, L_y$. We define a volume V_{ph-e} such that the boundary of this volume is offset by a distance Δr from the quantum well. By the definition of V_{ph-e}, we may consider electron–phonon processes in this volume as homogeneous in the $x-y$ plane and neglect fringe effects on the acoustic phonon emission.

In accordance with definition of Δr, the collision integral J_{ph-e} is equal to zero outside the volume V_{ph-e}. We integrate the kinetic equation (5) over the volume V_{ph-e}. The result of such an integration is given by the formula

$$\frac{\partial}{\partial t}\int_{V_{ph-e}}\frac{N_{\mathbf{q}}(\mathbf{r})}{V_{ph-e}}d\mathbf{r}+\oint_{S_{ph-e}}\mathbf{u}_{\mathbf{q}}\frac{N_{\mathbf{q}}(\mathbf{r})}{V_{ph-e}}d\mathbf{S}$$
$$=\Im_{ph-e}+\Im_{ph-ph}, \tag{6}$$

where S_{ph-e} is the surface which bounds the volume V_{ph-e}, the ratio $N_{\mathbf{q}}(\mathbf{r})/V_{ph-e}$ is the phonon distribution function normalized per unit volume, so the surface integral represents the flux of phonons with wave vector $\mathbf{q}$, and $\Im_{ph-e}$ and $\Im_{ph-ph}$ stand for integrated collision integrals J_{ph-e} and J_{ph-ph}, respectively. We assume that the length of phonon–phonon interaction is considerably larger than any dimension of the volume V_{ph-e}. For such materials as Si or GaAs, it is really the case for phonons with wavelength of the order of 100 Å. $\Im_{ph-e}$ is given by the formula

$$\Im_{ph-e}=\frac{4\pi}{\hbar}|\Gamma_q|^2\sum_{\mathbf{k}_\parallel,n,n'}\mathscr{I}(n',n,q_z)[(1-f_{n,\mathbf{k}_\parallel})$$
$$\times f_{n',\mathbf{k}_\parallel+\mathbf{q}_\parallel}+(f_{n',\mathbf{k}_\parallel+\mathbf{q}_\parallel}-f_{n,\mathbf{k}_\parallel})\ \sigma_{\mathbf{q},\mathbf{q}}]$$
$$\times\delta(\varepsilon_{n,\mathbf{k}_\parallel}-\varepsilon_{n',\mathbf{k}_\parallel+\mathbf{q}_\parallel}+\hbar\omega_q). \tag{7}$$

The term in Eq. (7) proportional to $\sigma_{\mathbf{q},\mathbf{q}}$ describes the processes of stimulated phonon emission and absorption. If the change in $\sigma_{\mathbf{q},\mathbf{q}}$ due to phonon emission and absorption by quasi-two-dimensional electron gas is small in comparison with the phonon density matrix in thermal equilibrium, we may substitute the Planck function $N^T_{\hbar\omega}$ for $\sigma_{\mathbf{q},\mathbf{q}}$ in Eq. (7).

From Eqs. (6) and (7) it follows that the energy flux of acoustic phonons with wave vectors in a domain $\Delta\mathbf{Q}$ emitted by quasi two–dimensional electrons is given by the formula

$$\Delta G=\frac{4\pi}{\hbar}\sum_{\mathbf{q}\in\Delta\mathbf{Q}}\hbar\omega_q|\Gamma_q|^2\sum_{\mathbf{k}_\parallel,n,n'}\mathscr{I}(n',n,q_z)$$
$$\times[(1-f_{n,\mathbf{k}_\parallel})f_{n',\mathbf{k}_\parallel+\mathbf{q}_\parallel}+(f_{n',\mathbf{k}_\parallel+\mathbf{q}_\parallel}-f_{n,\mathbf{k}_\parallel})N^T_{\hbar\omega}]$$
$$\times\delta(\varepsilon_{n,\mathbf{k}_\parallel}-\varepsilon_{n',\mathbf{k}_\parallel+\mathbf{q}_\parallel}+\hbar\omega_q). \tag{8}$$

From Eq. (8) and the definition of Eq. (1) we obtain the differential energy flux $\mathscr{G}(\hbar\omega,\Omega)$

$$\mathscr{G}(\hbar\omega,\Omega)=\frac{E_a^2q^4}{4\pi^2\rho u}\sum_{\mathbf{k}_\parallel,n,n'}\mathscr{I}(n',n,q_z)[(1-f_{n,\mathbf{k}_\parallel})$$
$$\times f_{n',\mathbf{k}_\parallel+\mathbf{q}_\parallel}+(f_{n',\mathbf{k}_\parallel+\mathbf{q}_\parallel}-f_{n,\mathbf{k}_\parallel})N^T_{\hbar\omega}]$$
$$\times\delta(\varepsilon_{n,\mathbf{k}_\parallel}-\varepsilon_{n',\mathbf{k}_\parallel+\mathbf{q}_\parallel}+\hbar\omega_q). \tag{9}$$

It is worth mentioning, that Eq. (9) takes into account both the phonon emission and phonon absorption processes. In addition, due to integration over the closed surface S_{ph-e} which bounds the volume of acoustic phonon interaction with quasi-two-dimensional electrons, Eq. (9) gives the differential energy flux in excess of the equilibrium differential energy flux, determined by the function $N^T_{\hbar\omega}$. It will be shown later, that the differential energy flux (9) is a strongly anisotropic function. This anisotropy enters Eq. (9) through the electron distribution function and through the overlap integral. The electron distribution function determines anisotropy in the $x-y$ plane, while the overlap integral determines anisotropy in respect to a spherical angle θ (the angle between the axis z and a given direction). The initial cause for anisotropy in the $x-y$ plane is the applied electric field which modifies the electron distribution function, and through this function it makes the phonon differential energy flux anisotropic in the $x-y$ plane.

Outside the volume V_{ph-e} the phonon kinetic equation has the form

$$\frac{\partial N_{\mathbf{q}}(\mathbf{r})}{\partial t}+\mathbf{u}_{\mathbf{q}}\frac{\partial N_{\mathbf{q}}(\mathbf{r})}{\partial\mathbf{r}}=J_{ph-ph}. \tag{10}$$

If the phonon decay due to phonon–phonon interactions and other possible mechanisms of scattering is small over the distance d from the quantum well to a phonon detector, the phonon propagation may be treated as ballistic and the approximation of the geometrical optics be employed. This condition is held for the samples used in experiments[1–8] (estimates are given in the next section). Therefore, the phonon energy detected by a sensor on a surface of the sample is the same as that determined by Eq. (9).

V. RESULTS OF NUMERICAL SIMULATION AND DISCUSSION

We have studied the acoustic phonon radiation patterns and the acoustic phonon emission spectra for the case of a nondegenerate electron gas. The restrictions which this imposes on the applicability of our results are not strict as long as we consider a heated electron gas. Appropriate estimates are considered in this section. Parameters of the materials are taken for a GaAs/AlGaAs double barrier heterostructure. The numerical results presented here correspond to the case where the lattice temperature is 30 K. At higher temperatures (e.g. at room temperature), optical phonon scattering dominates over other mechanisms and the equilibrium acoustic phonon population is too high to accurately resolve phonons emitted by quasi-two–dimensional electron gas. At very low lattice temperatures (e.g., 4.2 K) the electron gas degeneracy is more important and limits the applicability of our model. The width of the quantum well, a, is taken to be 100 Å. For this width, the second electron subband is approximately 150 meV above the first subband. It is substantially higher than the average electron energy, for this reason the second subband is practically unpopulated.

The kinetic equation for electrons takes into account all significant mechanisms of electron scattering in QW: electron scattering by acoustic phonons, as well as electron scattering by confined and interface optical phonons. We use the same Hamiltonians of electron interactions with optical phonons in a quantum well as given in Ref. 18. The electron–phonon collision integrals follow from these Hamiltonians. However, in electron collision integrals with phonons we take the equilibrium phonon distribution function assuming that the thermal bath is only slightly disturbed due to phonon emission by heated electrons. This is consistent with the assumption we made to obtain Eq. (8) from Eq. (7). We have solved the kinetic equation for electrons employing the Monte Carlo technique. The electron distribution function is approximated by an ensemble of a large number

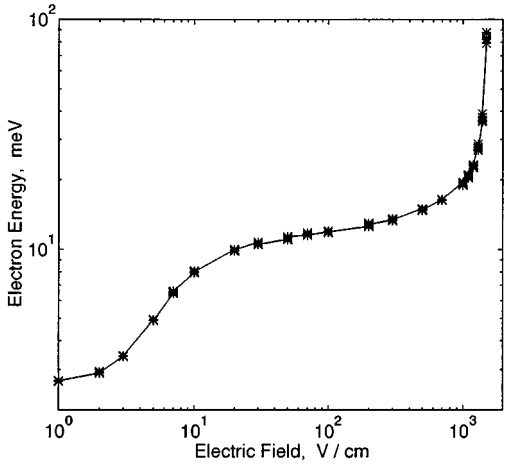

FIG. 2. The average electron kinetic energy as a function of the applied electric field. GaAs/AlAs quantum well, $T=30$ K, $a=100$ Å.

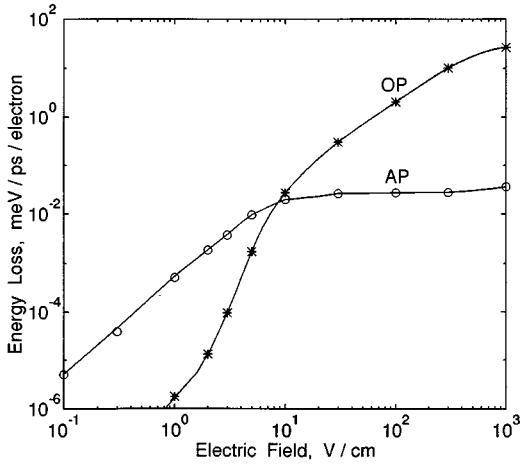

FIG. 3. The electron energy dissipated through acoustic phonon emission (marked AP) and through optical phonon emission (marked OP) per unit time, per one electron as a function of the applied electric field. GaAs/AlAs quantum well, $T=30$ K, $a=100$ Å.

of electrons (particles). We traced the trajectories of the particles in the phase space in a given electric field and scattered them to obtain a stationary distribution function. We used the standard Monte Carlo method for two-dimensional (2D) electrons as described in detail in Ref. 19. The electron distribution function obtained by this technique has been used to calculate the differential energy flux of Eq. (9). However, because $\mathcal{G}(\hbar\omega,\Omega)$ is a three-dimensional function of the spherical angles θ and ϕ, and the phonon energy $\hbar\omega$, all results will be presented as integrated over energies or solid angles functions $\mathcal{G}_{\hbar\omega}(\Omega)$ and $\mathcal{G}_{\Omega}(\hbar\omega)$, respectively.

The average electron energy as a function of the applied electric field is shown in Fig. 2. It allows us to analyze the applicability of the applied approach. The estimate for the electron Fermi energy in a GaAs QW is given by the formula $\varepsilon_F \approx 3.5\times(n_s/10^{11}\mathrm{cm}^{-2})$ meV, where n_s is the electron surface concentration. Then, for $n_s=10^{11}$ cm^{-2}, the electron gas may be considered nondegenerate if the electric field is 10 V/cm or higher.

We may mark two characteristic fields on Fig. 2 at which the curve for average energy bends. The first, E_1, is equal to 10 V/cm, and the second, E_2, is approximately equal to 10^3 V/cm. In the fields $E<E_1$ practically all the electron energy is dissipated through the acoustic phonon emission. The electron average energy grows linearly with the electric field. The saturation in the region of low fields of about 1 V/cm is due to the lower limit imposed by the thermal energy, which for the lattice temperature $T=30$ K is equal to 2.6 meV. In the range of electric fields $E_1<E<E_2$, a significant part of the electron energy is initially transferred to the optical phonons. The optical phonon emission, which is much stronger than the acoustic scattering, stabilizes the electron energy growth. In electric fields $E>E_2$ electrons run away from optical phonons. The electron energy dissipated through the acoustic phonon emission and through the optical phonon emission is shown on Fig. 3.

We have investigated the differential energy flux for acoustic phonons in the range of electric fields $E<E_2$. The optical phonons emitted in the case of strong electric fields $E_1<E<E_2$ are downconverted to acoustic phonons[20] with a energy of about 18 meV. These phonons may decay into lower energy phonons. However, for a realistic thickness of the substrate ($\approx$1 mm), the downconverted phonons and products of their decay may be discriminated from the phonons directly emitted by electrons, because their energies belong to different ranges. The mean free path of 1 mm (this is a typical thickness of the semiconductor substrate) corresponds to acoustic phonons with an energy of 9 meV. The energy dependence of the mean free path is inversely proportional to the fifth power of energy. Due to this strong energy dependence, all products of the optical phonon decay reach boundaries of the sample well before the phonon energy approaches the energy range of that directly emitted by electrons acoustic phonons.

The radiation patterns of quasi-two-dimensional electron gas in electric fields of 10, 100, and 1000 V/cm are shown on Fig. 4. To visualize the two–dimensional function $\mathcal{G}_{\hbar\omega}(\Omega)=\mathcal{G}_{\hbar\omega}(\theta,\phi)$, we fix an angle ϕ and plot a parametric curve $(|\mathcal{G}_{\hbar\omega}(\theta,\phi)|\sin\theta,\ \mathcal{G}_{\hbar\omega}(\theta,\phi)\cos\theta)$, $0<\theta<\pi/2$; $\theta=0$ corresponding to the z-direction, $\theta=\pi/2$ corresponds to a direction in the $x-y$ plane, namely the direction given by the unit vector $(\cos\phi,\sin\phi,0)$. The plots above the abscissa correspond to prevailing phonon emission (positive $\mathcal{G}_{\hbar\omega}(\theta,\phi)$), the plots below the abscissa correspond to prevailing phonon absorption (negative $\mathcal{G}_{\hbar\omega}(\theta,\phi)$). The spectra of the acoustic phonons given by the function $\mathcal{G}_{\Omega}(\hbar\omega)$ are shown on Fig. 5 for several electric fields.

Comparing curves on Fig. 4 we may conclude, that for $\phi\approx 0$ and the x–direction (the direction of the average electron velocity), the increase of the electric field from 10 to 1000 V/cm results in an increase of the maximum of $\mathcal{G}_{\hbar\omega}(\theta,0)$ by approximately two times (from 5.5×10^{-3} to 12×10^{-3} meV/(ps sr electron)). At the same time, for $\phi\approx 0$ and the z–direction, the maximum of $\mathcal{G}_{\hbar\omega}(\theta,0)$ is increased approximately 3.5 times (from 7.5×10^{-2} to 25×10^{-2} meV/(ps sr electron)). The absolute value of energy per unit solid angle, transmitted in the z-direction is an

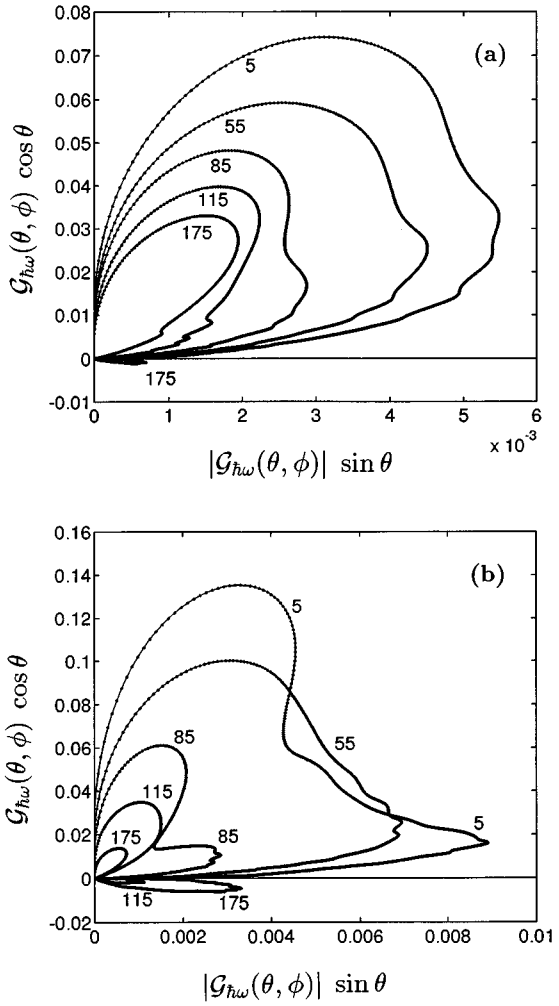

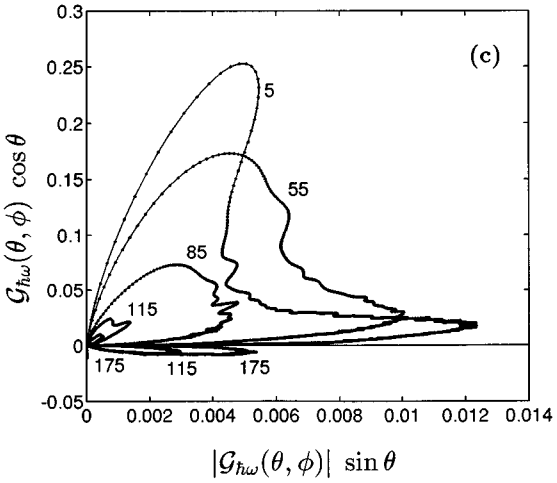

FIG. 4. Radiation pattern of acoustic phonons, $\mathcal{G}_{\hbar\omega}(\theta,\phi)$, in units meV/(ps sr electron) as a function of the angle θ for azimuthal angles $\phi = 5°$, 55°, 85°, 115°, 175°. The numbers at the curves correspond to the angles ϕ. GaAs/AlAs quantum well of width 100 Å, lattice temperature $T=30$ K. Electric field 10 V/cm (a), 100 V/cm (b), 1000 V/cm (c).

order of magnitude or more larger than the energy transmitted in the x-direction. There is well pronounced anisotropy of the phonon radiation in the $x-y$ plane; the acoustic phonons are emitted preferentially in the direction of the average electron velocity. For ϕ close to π and some angles θ acoustic phonon absorption exceeds emission and the resultant differential energy flux $\mathcal{G}_{\hbar\omega}(\theta,\phi)$ is negative (parts of curves below the abscissa). In addition, the radiation patterns, $\mathcal{G}_{\hbar\omega}(\theta,\phi)$, have many details.

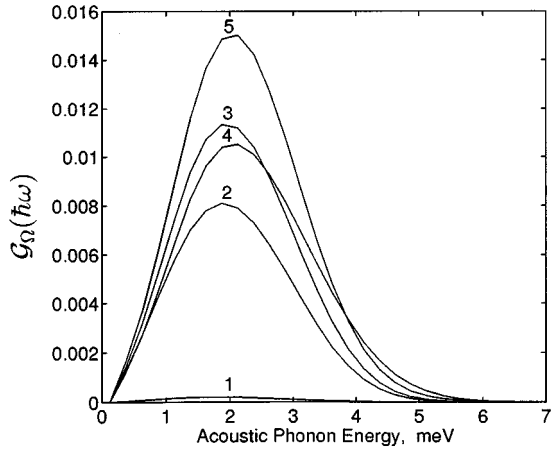

FIG. 5. The spectra of the acoustic phonon energy flux, $\mathcal{G}_\Omega(\hbar\omega)$, in units 1/(ps electron) for electric fields 1 V/cm (1), 10 V/cm (2), 100 V/cm (3), 300 V/cm (4), and 1000 V/cm (5). GaAs/AlAs quantum well, $T=30$ K, $a=100$Å.

A simple estimate cannot explain so strong a radiation pattern anisotropy. The z-component of the phonon wave vector in Eq. (9) is determined by the overlap integral $\mathcal{I}(1,1,q_z)$. It is given in Fig. 1. Therefore, the typical q_z is approximately $2\pi/a$. For a 100 Å wide quantum well it is equal to 6×10^6 cm^{-1}. A typical in-plane wave vector of phonon emitted by a 20 meV electron is equal to 3×10^6 cm^{-1}. This anisotropy is much smaller, than shown in Fig. 4.

There are two major factors which contribute to the angular dependence of the radiation pattern. The first is the radiation pattern of a single electron. The second is the shape of the electron distribution function, which averages the radiation patterns of individual electrons. Let us consider the radiation pattern of a single electron in the lowest subband. It can be obtained from Eq. (9) if we take the electron distribution function in the form $f_{n,\mathbf{k}_\parallel}=\delta_{n,1}\delta_{\mathbf{k}_\parallel,\mathbf{k}_\parallel^{(0)}}$. The radiation pattern for the 30 meV electron is given on Fig. 6. Fig. 6(a) is a significantly magnified part of Fig. 6 (b). The meaning of the curves is slightly different from

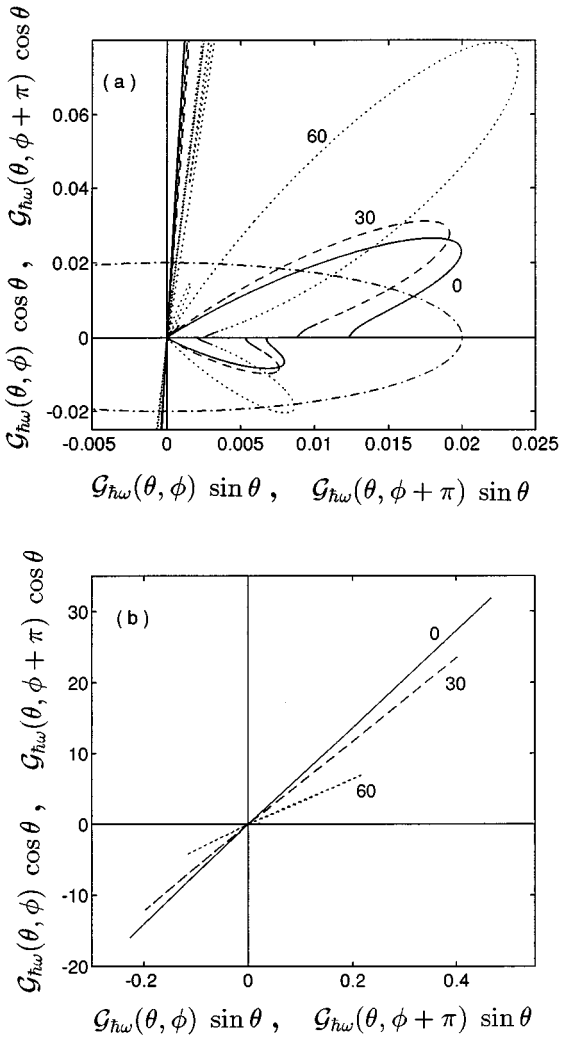

FIG. 6. Radiation pattern of an individual electron with energy 30 meV, $\mathcal{G}_{\hbar\omega}(\theta,\phi)$, in units meV/(ps sr) as a function of the angle θ for several azimuthal angles ϕ. Cross–sections of the surface $\mathcal{G}_{\hbar\omega}(\theta,\phi)$ by the plane $\phi=0°$ (solid line), $\phi=30°$ (dashed line), $\phi=60°$ (dotted line) are shown. The numbers at the curves correspond to the angles ϕ. GaAs/AlAs quantum well, $T=30$ K, $a=100$ Å. (a) zoom in; (b) zoom out. The dash–dotted line is used to draw a curve of the constant function $\mathcal{G}_{\hbar\omega}(\theta,\phi)$.

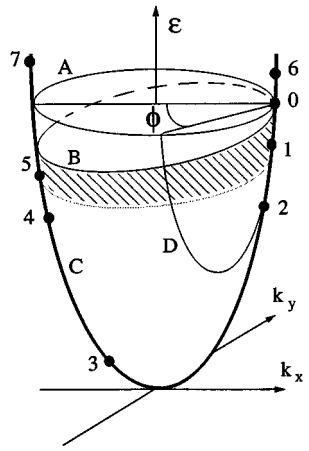

FIG. 7. Diagram of the lowest electron subband $\varepsilon(k_x,k_y)$. The initial state of the electron is marked by 0. Possible electron final states are marked by numbers 1 through 5 for the case of phonon emission and numbers 6 and 7 for the case of phonon absorption. Possible final states for a given angle ϕ of emitted phonons lie in the curves marked by letters C and D. Possible electron final states after acoustic phonon emission with the maximal electron energy lie in the curve marked B. The circle marked by the letter A is a cross-section of the paraboloid by the plane of equal energy.

that which was used in Fig. 4. We make an imaginary plot of the surface defined in parametric form as $(\mathcal{G}_{\hbar\omega}(\theta,\phi)\sin\theta\cos\phi, \mathcal{G}_{\hbar\omega}(\theta,\phi)\sin\theta\sin\phi, \mathcal{G}_{\hbar\omega}(\theta,\phi)\cos\theta)$, $0<\theta<\pi/2$, $-\pi<\phi<\pi$ and then make a cross–section by a plane which makes an angle ϕ with the axis x and includes the axis z. Therefore, for a given ϕ, curves in the first quadrant correspond to positive $\mathcal{G}_{\hbar\omega}(\theta,\phi)$ and curves in the third quadrant correspond to negative $\mathcal{G}_{\hbar\omega}(\theta,\phi)$. Curves in the second and fourth quadrants correspond to positive and negative $\mathcal{G}_{\hbar\omega}(\theta,\phi)$ respectively, however, the polar angle ϕ should be replaced by $\phi+\pi$.

We will explain the radiation pattern of Fig. 6 using the diagram on Fig. 7. Let us consider possible electron transitions from an initial state ''0'' (Fig. 7) due to acoustic phonon emission. The circle ''*A*'' represents a cross–section of the paraboloid by the plane $\varepsilon=const$, the curve ''B'' represents all possible final states of the electron, which has emitted acoustic phonon with $q_z=0$. The shaded area below the curve ''B'' represents possible final states of the electron, which has emitted an acoustic phonon with arbitrary q_z. The height of this area is determined by the overlap integral. From Fig. 1, the maximum q_z is approximately equal to $4\pi/a$, therefore the shaded area height is equal to $4\pi\hbar u/a$.

Let us fix the angle ϕ, so that $\phi=0$. Then all possible final states for the electron lie on the parabola ''C,'' i.e. the intersection of the paraboloid of $\varepsilon=\varepsilon(k_x,k_y)$ and the plane (ε,k_x). Now we trace the change in the radiation pattern, when we move the electron final state through points ''1,'' ''2,'' ''3,'' ''4,'' and ''5.'' Note, that these points correspond to sequentially increasing angle θ. Electron transitions from ''0'' to ''1'' correspond to the acoustic phonon emission with θ close to zero. They result in the largest peak in the first quadrant on Fig. 6. The electron scatterings from ''0'' to ''2,'' ''3,'' and ''4'' correspond to acoustic phonon emissions with sequentially larger θ. However, the probabilities of those processes are almost zero as a result of the too large values of the corresponding q_z. The quasi conservation of the phonon q_z defined by the overlap integral limits the electron transitions within the shaded area on Fig. 7. For this reason, we practically do not have radiation on Fig. 6 for some range of θ corresponding to electron transitions from ''0'' to ''2,'' ''3,'' and ''4.'' The electron transitions from ''0'' to ''5'' fall within a range of allowed q_z (shaded area on the diagram) and these electron transitions give a second peak in the first quadrant. From the geometry of Fig. 7 it is clear that on the θ scale the first peak (transitions ''0'' → ''1'') is much more narrow, than the second peak (transitions ''0'' → ''5''). At the same time, the scattering rates ''0'' → ''1'' and ''0'' → ''5'' are practically the same, because they are determined by the total phonon wave vectors q, which are almost the same due to large q_z. For this reason,

the phonon energy irradiated to the first peak and to the second peak are almost the same. As a consequence, the first peak is much larger than the second.

Between the two just discussed strong maxima of the radiation pattern in the first quadrant of the Fig. 6, there are several small maxima. They resulted from oscillations of the overlap integral (see Fig. 1).

The maxima in the third and the fourth quadrants on Fig. 6 are due to acoustic phonon absorption (as is explained above, we plot the negative $\mathscr{G}_{\hbar\omega}(\theta,\phi)$ below the abscissa). The peak in the third quadrant corresponds to electron transitions from ''0'' to ''6''; the peak in the fourth quadrant corresponds to electron transitions from ''0'' to ''7.'' It is assumed that both ''6'' and ''7'' final states are within a range of allowed q_z, as determined by the overlap integral.

If the angle between electron and phonon wave vectors, ϕ, is not equal to zero, the electron final states lie on the cross–section of the paraboloid $\varepsilon=\varepsilon(k_x,k_y)$ and the plane, which is perpendicular to the (k_x,k_y) plane, goes through the point ''0,'' and make the angle ϕ with the plane (ε,k_x) (the curve ''*D*'' on Fig. 7). The analysis of the radiation pattern for $\phi \neq 0$ can be done in the same fashion as it was done for $\phi=0$. It is obvious, that positions of maxima in θ space should depend on ϕ. Such dependence is shown on Fig. 6(b). Moreover, if the ϕ is close to $\pi/2$ and/or electron energy is small, the maxima of the radiation pattern become broader (in terms of θ) and may merge.

The radiation patterns of individual electrons are averaged over the electron distribution function. We will give only a qualitative description for the electron distribution function transformation when the electric field increases in the range $0<E<1000$ V/cm. Important information for the average electron energy change is given in Fig. 2. The electric field growth from 0 to 10 V/cm results in electron gas heating, while the electron distribution function remains close to a displaced Maxwellian function. The radiation pattern $\mathscr{G}_{\hbar\omega}(\theta,\phi)$ for the electric field $E=10$ V/cm is given on Fig. 4 (a). It is slightly asymmetric in the $x-y$ plane. However, the radiation patterns for individual electrons are substantially smeared due to stochastic motion of electrons.

Electric fields from approximately 50 V/cm to 200 V/cm correspond to the streaming regime. The vast majority of electrons have their energies below the optical phonon threshold and perform quasi-periodic motion in $\mathbf{k}_{\|}-$space. The electron distribution is strongly asymmetric, it is stretched along the direction of the electric field. The radiation pattern of phonons for $E=100$ V/cm is given on Fig. 4 (b). It is strongly asymmetric in the $x-y$ plane.

For the electric fields close to the run-away threshold (which is slightly larger than 1000 V/cm), a significant number of electrons have energies notably above the optical phonon threshold. The electron distribution function is asymmetric in the $x-y$ plane and stretched along the *x*-axis, however it is substantially broader in both *x*- and *y*-directions, than for $E=100$ V/cm. The radiation pattern of phonons for $E=1000$ V/cm is given on Fig. 4 (c). It is also strongly asymmetric in the $x-y$ plane. The radiation patterns for $\phi=0$ in the electric fields 100 V/cm and 1000 V/cm carry features of the individual electron radiation pattern, they have two major peaks for two different θ. This is due to stretched shapes of the distribution functions.

In spite of the significant modification of the electron distribution function and the phonon radiation patterns when the electric field grows, the spectrum of irradiated phonons remains remarkably unchanging (see Fig. 5). The average energy of the phonons is determined by the width of the quantum well and is approximately equal to $2\pi\hbar u/a$. The position of the maxima may be changed only if both the lattice temperature and the electric field are so low, that the average electron energy is smaller than $2\pi\hbar u/a$. Equation (9) gives the differential phonon energy flux in excess of the thermal equilibrium background determined by $N^T_{\hbar\omega}$. Therefore, the total energy of the irradiated phonons is equal to zero if $E=0$. It grows in small electric fields and then become almost field independent (see Fig. 3). It happens because the average phonon energy does not depend on the electric field, and the electron–acoustic phonon scattering rate in one electron subband 2D case is also almost constant due to energy independent density of states.

VI. CONCLUSIONS

We have analyzed the acoustic phonon radiation emitted by quasi-two–dimensional electrons in double barrier quantum well structures. We have included effects of the non-equilibrium electron distribution and stimulated emission processes. As a result, we have obtained strong asymmetry for the radiation pattern in the plane of the quantum well for the case where the electric field is strong enough. The radiation pattern of a quasi-two-dimensional electron gas has strong anisotropy which has been explained in terms of radiation patterns of the individual electrons and the electron distribution function.

ACKNOWLEDGMENTS

This work was supported by ARO. One of the authors (N.B.) would like to thank Dr. F. Vasko for helpful discussions on boundary conditions for the phonon density matrix.

[1] M. Rosenfusser, L. Köster, and W. Dietsche, Phys. Rev. B **34**, 5518 (1986).
[2] L. J. Challis, G. A. Toombs, and F. W. Sheard, *Physics of Phonons*, edited by T. Paszkiewicz (Springer, New York, 1987), pp. 348–374.
[3] L. J. Challis, A. J. Kent, and V. W. Rampton, Semicond. Sci. Technol. **5**, 1179 (1990).
[4] P. Hawker, A. Kent, O. Hughes, and L. Challis, Semicond. Sci. Technol. **7**, B 29 (1992).
[5] J. K. Wigmore, M. Erol, M Sahraoui-Tahar, C. Wilkinson, J. H. Davies, and C. Stanley, Semicond. Sci. Technol. **6**, 837 (1991).
[6] J. K. Wigmore, M. Erol, M. Sahraoui-Tahar, M. Ari, C. Wilkinson, J. Daviest, M. Holland, and C. Stanley, Semicond. Sci. Technol. **8**, 322 (1993).
[7] B. Danilchenko, A. Klimashov, S. Roshko, and M. Ashe, Phys. Rev. B **50**, 5725 (1994).
[8] M. Ashe, R. Heg, H. Kostial, B. Danilchenko, A. Klimashov, and S. Roshko, Phys. Rev. B **51**, 7966 (1995).
[9] F. T. Vasko, Sov. Phys. Solid State **30**, 1207 (1988).
[10] S. M. Badalian and Y. B. Levinson, Sov. Phys. Solid State **30**, 1592 (1988).
[11] S. M. Badalian and Y. B. Levinson, Phys. Lett. A **140**, 62 (1989); **155**, 200 (1991).

[12] F. T. Vasko, O. G. Balev, and P. Vasilopoulos, Phys. Rev. B **47**, 16 433 (1993).
[13] W. Xu and J. Mahanty, J. Phys.: Condens. Matter **6**, 6265 (1994).
[14] R. Mickevičius, V. Mitin, and V. Kochelap, J. Appl. Phys. **77**, 5095 (1995).
[15] V. V. Mitin, G. Paulavičius, and N. A. Bannov, Proceedings of the Ninth International Conference on Hot Carriers in Semiconductors, Chicago, IL, 31 July –4 August, 1995 (unpublished).
[16] V. Narayanamurti, Science **213**, 717 (1981).
[17] W. M. Gancza and T. Paszkiewicz, Comput. Phys. Commun. **85**, 42 (1995).
[18] N. Mori and T. Ando, Phys. Rev. B **40**, 6175 (1989).
[19] C. Jacoboni, *The Monte Carlo Method for Semiconductor Device Simulation* (Springer, New York, 1989); *Monte Carlo Device Simulation: Full Band and Beyond*, edited by K. Hess (Kluwer, Boston, 1991); K. Tomizawa, *Numerical Simulation of Submicron Semiconductor Devices* (Artech House, Boston, 1993).
[20] S. Tamura, Phys. Rev. B **31**, 2574 (1985); **48**, 13 502 (1993).